Structural characterization of dense reduced $BaTiO_3$ and $Ba_{0.95}La_{0.05}TiO_3$ nanoceramics showing colossal dielectric values

Z. Valdez-Nava [a], C. Tenailleau [a],*, S. Guillemet-Fritsch [a], N. El Horr [a], T. Lebey [b], P. Dufour [a], B. Durand [a], J.-Y. Chane-Ching [a]

[a] CIRIMAT, Université Paul Sabatier, 118 Route de Narbonne, 31062 Toulouse Cedex 9, France
[b] LAPLACE, Université Paul Sabatier, 118 Route de Narbonne, 31062 Toulouse Cedex 9, France

ABSTRACT

$BaTiO_{3-x}$ and $Ba_{0.95}La_{0.05}TiO_{3-x}$ nanoceramics showing colossal permittivity values have been characterized. While starting powders are of cubic symmetry, X-ray and Neutron Diffraction techniques and Raman Spectroscopy measurements show that the one-step processed ceramics obtained by Spark Plasma Sintering (SPS) contain cubic and tetragonal phases. Rather large oxygen deficiency determined in such ceramics by Electron Micro Probe analysis and Electron Energy Loss Spectroscopy analyzes is explained by the presence of Ti^{3+}, as evidenced by X-ray Photoelectron Spectroscopy measurements. Transmission Electron Microscopy and High Resolution Transmission Electron Microscopy show that these ceramics contain 50–300 nm grains, which have single-domains, while grain boundaries are of nanometer scale. Colossal permittivity values measured in our dense nanoceramics are explained by a charge hopping mechanism and an interfacial polarization of a large number of polarons generated after sample reduction in SPS apparatus.

1. Introduction

Perovskite-based materials form an important class of dielectric compounds since some can exhibit very high permittivity values that prompted numerous studies into the development of useful devices for microelectronics [1–4]. Indeed, high permittivity values in ceramics are essential for commercially used thermistors, capacitors and memory devices [5,6]. For several decades, $BaTiO_3$, of perovskite structure, and derived materials have incurred many scientific investigations in order to understand better and control the electrical properties of such dielectric materials with respect to their structural characteristics [7–10].

Stoichiometric cubic perovskite of ABO_3-type (A=alkaline-earth element and B=transition metal) contains A sites with cubic environments of oxygen while B sites are in an octahedral environment with corner-linked octahedra along all three independent crystallographic directions. The A sites thus occupy the free spaces left by the octahedra. Above the Curie temperature, T_c, the material is centrosymmetric and paraelectric. Below T_c, the material is non-centrosymmetric. The crystal cell distortion drives to the octahedra deformation and creates a separation between oppositely charged ion centres. The off-centred ions create an elementary dipole in each crystal cell, mobile with an external electric field (ferroelectric sample) and the material can become piezoelectric if polarized with mechanical constraints. Tetragonal symmetry implies such crystal distortion. In a $BaTiO_3$ single crystal for instance, Ti^{4+} is then slightly off-centred along the c direction and can vibrate more easily in the (a, b) plane, with $\varepsilon_a > \varepsilon_c$ [11]. Ferroelectric properties observed in tetragonal/cubic phases of barium titanate oxides and the Internal Barrier Layer Capacitor (IBLC) concept can explain some of the electrical characteristics of materials. But the so-called colossal values observed in a wide range of materials including those under study are not due to the geometry of the region responsible for them. In ceramics, the dielectric constant is also dependent on other factors such as the sample density, grain size and impurities. Therefore, dense ceramics, without impurities and of homogeneous microstructure and optimized small grain size present the highest dielectric constant.

The doping effects of La^{3+} on $BaTiO_3$ with respect to the structural and physical properties have been extensively studied over the past decades in order to improve $BaTiO_3$ dielectric properties [12]. Ba^{2+} ($r=1.35$ Å, according to Shannon's table [13]) substitution by La^{3+} ($r=1.032$ Å [13]) brings more electrons into the system, decreases the T_c, increases the dielectric constant up to a critical doping level and the material changes from insulator to n-type semiconductor and back to insulator. Morrison et al. [14] suggested that the electronic contribution induced by La-doping can be charge compensated by B cation vacancy and/or reduction while creating oxygen vacancies under low PO_2 and thus should be responsible for semiconductivity. The minimum of resistivity measured in coarse-grained and reduced La-doped $BaTiO_3$ samples, with

* Corresponding author. Tel.: +33 561556283; fax: +33 561556163.
E-mail address: tenailleau@chimie.ups-tlse.fr (C. Tenailleau).

0.01 < at%La < 0.10, was first explained by the passage from an ionic to electronic compensation [15]. It seems now established that the increase in resistance with increase in La content is more likely due to sample reoxidation upon cooling.

We have recently measured colossal permittivity values in ultra-fine grain size $BaTiO_{3-x}$ and La-doped $BaTiO_{3-x}$ ceramics prepared by a single-step process in a Spark Plasma Sintering (SPS) apparatus available in Toulouse [16]. The present paper is a detailed study of the structural characteristics of nanoceramics with two different compositions, each of them sintered at two temperatures, which gives an insight into the origin of the observed phenomenal electrical features.

2. Experimental and characterization techniques

Stoichiometric proportions of raw powders of $BaCl_2 \cdot 2H_2O$, $TiCl_3$ and $LaCl_3 \cdot 7H_2O$ (Prolabo) were used for the synthesis of $BaTiO_3$ and $Ba_{0.95}La_{0.05}TiO_3$ powders following an oxalate precipitation route described elsewhere [17]. Oxides were formed after calcination at 850 °C for 4 h in static air. Heating in a SPS apparatus is created by a current going through the whole sample placed in a conductive matrix and under an axial pressure. The main advantages in comparison with the conventional sintering method are to lower the temperature, decrease considerably the experimental time and obtain a very high densification with small grain sizes. The powders were introduced in the 8 mm internal diameter graphite die and placed under vacuum (4 Pa). The temperature was measured using a K thermocouple inserted within the matrix and close to the sample. The powders were sintered under 50 MPa for 3 min between 1050 and 1210 °C (50 °C/min heating rate), depending on the sample composition, followed by rapid cooling, using the Sumimoto 2080 SPS system available at the PNF2 CNRS platform at the University of Toulouse, France. Each thermal cycle took about 25 min.

Room temperature X-ray diffraction (XRD) measurements were systematically performed on powders and sintered ceramics using a Bruker D4 powder diffractometer ($CuK\alpha_{1,2}$ radiation, 40 kV and 40 mA). Raman spectroscopy (LabRAM HR800 high resolution Raman microscope, with a He–Ne laser at a wavelength of 632.82 nm) was used in the 100–1000 cm^{-1} range at room temperature to probe the local crystallographic structure and symmetry changes. Pellets ($\sim$3.2 g) of freshly SPS treated and reoxidized in air at 850 °C for 20 h $Ba_{0.95}La_{0.05}TiO_{3-x}$ ceramics were ground and measured simultaneously with 200 μA on the Polaris instrument at ISIS in UK. Backscattering detector banks data were then refined with the FULLPROF program using the Rietveld method. Scale factor, instrument correction parameters (Dtt1 and Dtt2), five coefficients background, profile factors (Sig1, Gam1, Gam2), cell parameters, atomic positions, isotropic factors and oxygen occupancies were refined for the main phase while only the scale factor and lattice parameters were refined for the minor phase.

The particle size and morphology of the products were analyzed by bright-field Transmission Electron Microscopy (TEM, JEOL, JEM 2010) and High Resolution Transmission Electron Microscopy (HRTEM, JEOL, JEM 2100F). Elemental analysis of the powders was determined using inductively coupled plasma (ICP) emission spectroscopy while chemical composition of the ceramics were analyzed with an Electron Micro Probe Analyzer (EMPA) using a CAMECA SX-100 instrument. Electron Energy Loss Spectroscopy (EELS) was used to verify chemical composition in ceramics by TEM with a Philips CM20 and a Gatan EELS measurement device (1 mm entrance diaphragm and 0.2 eV energy dispersion) using a 75 nm spot size. Samples were previously ground in ethanol before dispersion on copper grids. EELS measurements were also made for qualitative chemical distribution profiles on ceramics using a 2.75 nm spot size and a total analyzed length of 282 nm. No correction was applied for multiple scattering contributions. X-ray Photoelectron Spectroscopy (XPS) was performed on freshly fractured materials with a VG Escalab 220iXL apparatus for Ti oxidation states determination.

Relative permittivity and dielectric losses were measured with a HP4194A Impedance/Gain-Phase Analyzer in the range from 100 Hz to 1 MHz at room temperature, and from 123 to 373 K with a Novocontrol Alpha-A broadband spectrum analyzer coupled with a Quatro Cryosystem.

3. Results and discussion

Fig. 1 shows XRD patterns of $BaTiO_{3-x}$ and La-doped materials before and after SPS treatment. Very fine powders are of cubic structure at room temperature. Small extra peaks observed in $BaTiO_{3-x}$ samples were assigned to $BaTi_2O_5$ impurity phase. Fig. 2 shows TEM images of powders prepared from oxalate precursors and heated at 850 °C. The median grain size in both composition phases is 50 nm. This size is consistent with cubic symmetry [18]. Dense materials (above 97% relative density) were of a dark bluish color after the SPS treatment in reducing atmosphere due to a rich graphite environment. This color was not attributed to the graphite reaction with samples as FTIR measurements (Nicolet 510P analyzer) of CO_2 gas produced by a ceramic heated up to 1000 °C in air revealed a maximum residual carbon concentration of 100 ppm. However, the color change can easily be justified by the oxygen deficiency and formation of Ti^{3+} ([10] and see below). $BaTiO_{3-x}$ and 5% La-doped ceramics sintered at 1050 °C by the SPS method exhibit median grain size of 300 and 70 nm, respectively (see Fig. 2). Depending on the composition, SPS pellets prepared at higher temperature present larger grain size (300 nm for $Ba_{0.95}La_{0.05}TiO_{3-x}$ sintered at 1210 °C, for instance). From XRD data, comparison between (1 1 1) peak width and position at $2\theta \sim 38°$ and (0 0 2) associated with (2 0 0) peaks around 45° in 2θ shows that a phase of tetragonal symmetry is predominant in all ceramics with a cubic (or pseudo-cubic) phase (see insets of Fig. 1). This is in agreement with previous results showing coexistence of both phases after using the SPS technique [19]. Peak broadening and intensity variations associated with the change of powder to
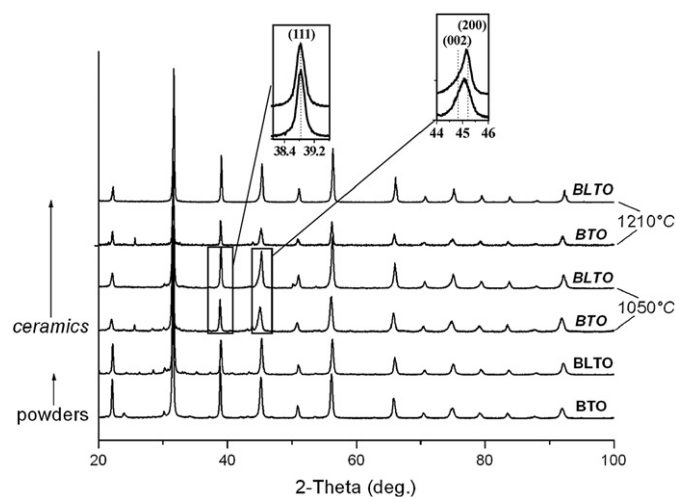

Fig. 1. XRD patterns of undoped (BTO), 5% La-doped (BLTO) $BaTiO_3$ powders and corresponding SPS-prepared ceramics. Insets show that tetragonal symmetry is present in ceramics, for instance, due to separation of (0 0 2) and (2 0 0) peaks with single (1 1 1) peak, the latter being characteristic of cubic-like phase.
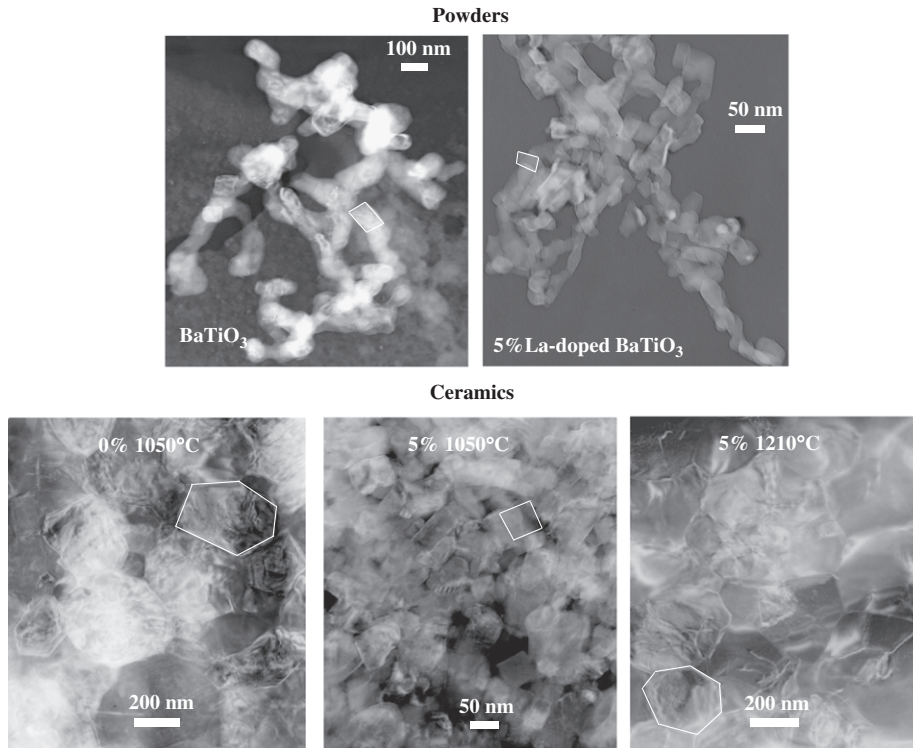
Fig. 2. TEM images of $BaTiO_3$ and $Ba_{0.95}La_{0.05}TiO_3$ powders (top left and right, respectively) prepared by the oxalate route. Median grain size is around 50 nm for both samples. TEM images on ion beam thinned $BaTiO_{3-x}$ and $Ba_{0.95}La_{0.05}TiO_{3-x}$ nanoceramics sintered at 1050 °C (bottom left and middle, respectively) and $Ba_{0.95}La_{0.05}TiO_{3-x}$ obtained at 1210 °C (bottom right). Lines are indicators for the eyes.

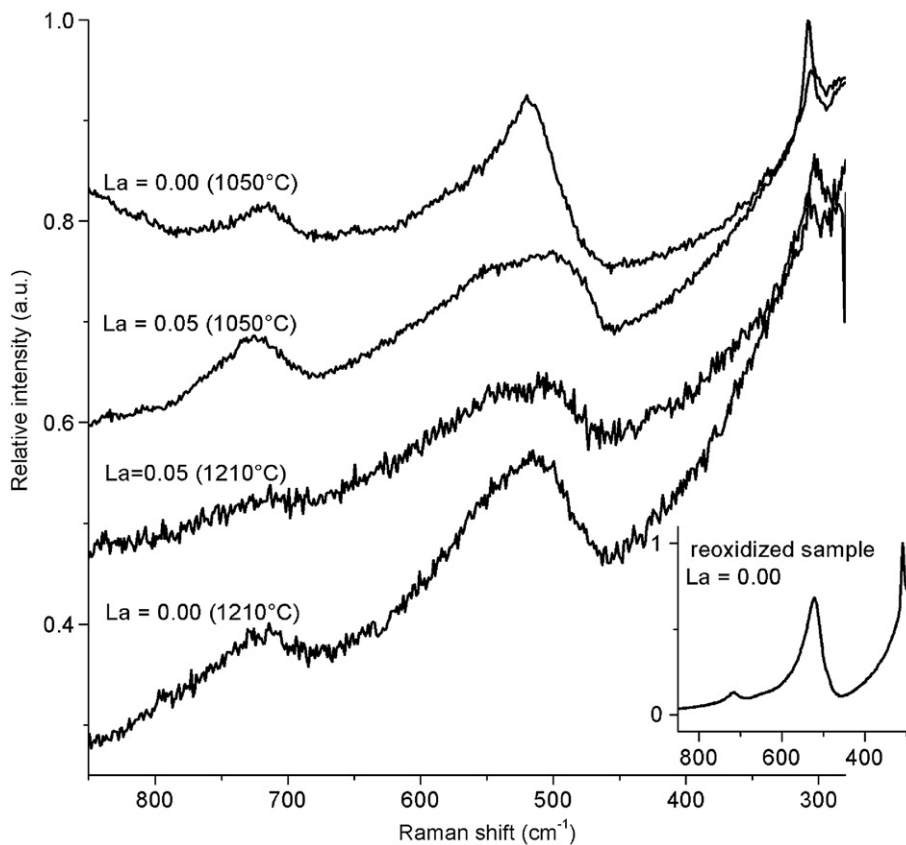**Fig. 3.** Raman spectra of single-step SPS processed $BaTiO_{3-x}$ and $Ba_{0.95}La_{0.05}TiO_{3-x}$ ceramics. Inset shows a Raman spectrum of reoxidized sample in air.

ceramic indicate a decrease in crystallinity after sintering and rapid cooling by the SPS method. A small grain size and/or reduced tetragonality ($c/a = 1.006$ for both materials at room temperature, where a and c are the lattice parameters with P4mm space group) is usually responsible for peak broadening observed in the XRD patterns. Raman scattering spectra of the ceramics at room temperature also confirm the presence of the two phases with two peak maxima at 518 and 720 cm^{-1} characteristics of cubic and tetragonal symmetries, respectively (Fig. 3) [20,21]. A broad peak at $\sim$280 cm^{-1} is also attributed to the cubic phase while a weak peak at $\sim$305 cm^{-1} corresponds to the tetragonal phase.

In the present study, all BaTiO$_{3-x}$ and 5% La-doped ceramics exhibit a tetragonal phase. For the two ceramics sintered at 1050 °C, the a and c cell parameters of the tetragonal phase ($a = 4.0080(3)$ and $c = 4.0324(4)$ Å for the BaTiO$_{3-x}$ phase at RT) decrease by 0.010(1) and 0.004(1) Å upon doping, respectively. This contraction is explained by the occupation of a smaller A cation in between the B site octahedral environments. Due to symmetry and lattice distortion, nanograins in such ceramics are therefore composed of a large number of spontaneous dipoles. If all dipoles are aligned along a preferential direction for each small domain, oxygen and Ti vacancies may frustrate Ti free oscillation within its octahedron under electric field but favor ferroelectric domain reorientation by separating corner-shared octahedra. The small presence of Ti^{3+} ($r = 0.670$ Å [13]) detected by XPS in our reduced materials and replacing Ti^{4+} ($r = 0.605$ Å [13]), with Ti^{3+}/Ti$^{4+} < 4\%$ in all ceramics, would rather tend to moderate Ti mobility. However, the cubic phase observed in these ceramics interferes with long-range tetragonal order providing more freedom for each B site octahedral environment to adjust when an electric field is applied. The EMPA technique was used on 40×40 μm^2 homogeneous ceramic area in order to determine the elementary composition. TiO$_2$, BaSO$_4$ and La glass were used as standards. Ba/Ti and O/Ti ratios were 0.93(3) and 2.62(9) for all samples based on BaTiO$_{3-x}$ and Ba$_{0.95}$La$_{0.05}$TiO$_{3-x}$ formulae, respectively. Although the latter ratio is synonymous of a rather large oxygen deficiency, EELS measurements performed on freshly fractured samples seemed to confirm the x values, with an O/Ti ratio equal to 2.64(2). Global electroneutrality proposes that Ba^{2+}=La^{3+}+e$^-$, Ti^{4+}+e$^-$=Ti^{3+} and O^{2-}=½O$_2$+V$_O$+2e$^-$ are the only possible reactions. A 4 at% Ti^{3+} maximum value as obtained by XPS implies a stoichiometric repartition of elements with $x \sim 0$. Ti^{3+}/Ti$^{4+} \sim 2/3$ ratio would be required for a general Ti$^{3.35+}$ oxidation state, with $x \sim 0.3$ as determined by EPMA and EELS. The presence of Ti vacancies can also be considered as possible in materials sintered under drastic reducing atmosphere. Oxygen deficiency in Ba$_{0.95}$La$_{0.05}$TiO$_{\sim 2.7}$ (with Ti$^{3.35+}$) could mean that $\sim$15 at% V$_{Ti}$ or 9 at% V$_{Ti}^{4+}$ is present for Ti^{3+}/Ti$^{4+} \sim 4\%$. West [2] and Sinclair et al. [10] have examined BaTiO$_3$-type materials that exhibit Ti vacancies or oxygen concentration corresponding to a 0.15 maximum x value. Strongly reduced epitaxial BaTiO$_{3-x}$ thin films with x as high as 0.48 have been characterized [22]. However, spectroscopic techniques such as EELS and XPS usually provide more information about the analyzed surface of a sample than the bulk. EELS is very well suited for relatively low atomic numbers, where the excitation edges tend to be sharp, well-defined and at experimentally accessible energy losses. EELS allows quick and reliable measurement of local thickness in transmission electron microscope. Within transmission EELS, the technique can measure plasmons and interband transitions and/or inner-shell ionizations, which provides the same information as X-ray absorption spectroscopy, but from much smaller volumes of material. XPS spectra relate to the energies of the photoelectrons by measuring simultaneously the kinetic energy and number of electrons that escape from the top 1 to 10 nm of the material being analyzed. Thus use of complementary characterization techniques is required in order to elucidate the oxygen deficiency. TGA measurements (TAG Setaram 92 instrument) performed on

30 mg of reduced material after the SPS treatment up to 900 °C (3 °C/min heating rate) in blowing air did not show evidence for the expected gain mass associated with sample reoxidation. These results tend to show that oxygen deficiency measured by spectroscopic techniques is most likely over estimated. But TGA is not conclusive in this case as these similar oxidations are often sluggish. Raman spectroscopy showed that both cubic and tetragonal phases still coexist in reoxidized samples but a comparison between the peak intensities show that the amount of the remaining cubic phase is smaller (see inset in Fig. 3). While Rietveld refinements on neutron powder diffraction data of ground Ba$_{0.95}$La$_{0.05}$TiO$_{3-x}$ nanoceramics just after the SPS treatment and following oxidation in air at 850 °C for 50 h showed similar stoichiometric oxygen occupancies, they confirmed the disappearance of the cubic phase with values of 10.8(3) and 2.3(2) wt% (Fig. 4).

Colossal permittivities, $\varepsilon \sim 0.8 \times 10^6$ (with tan $\delta \sim 0.6$), were measured at room temperature and 1 kHz in frequency for BaTiO$_{3-x}$ nanoceramics sintered at 1050 °C by the SPS technique, for instance
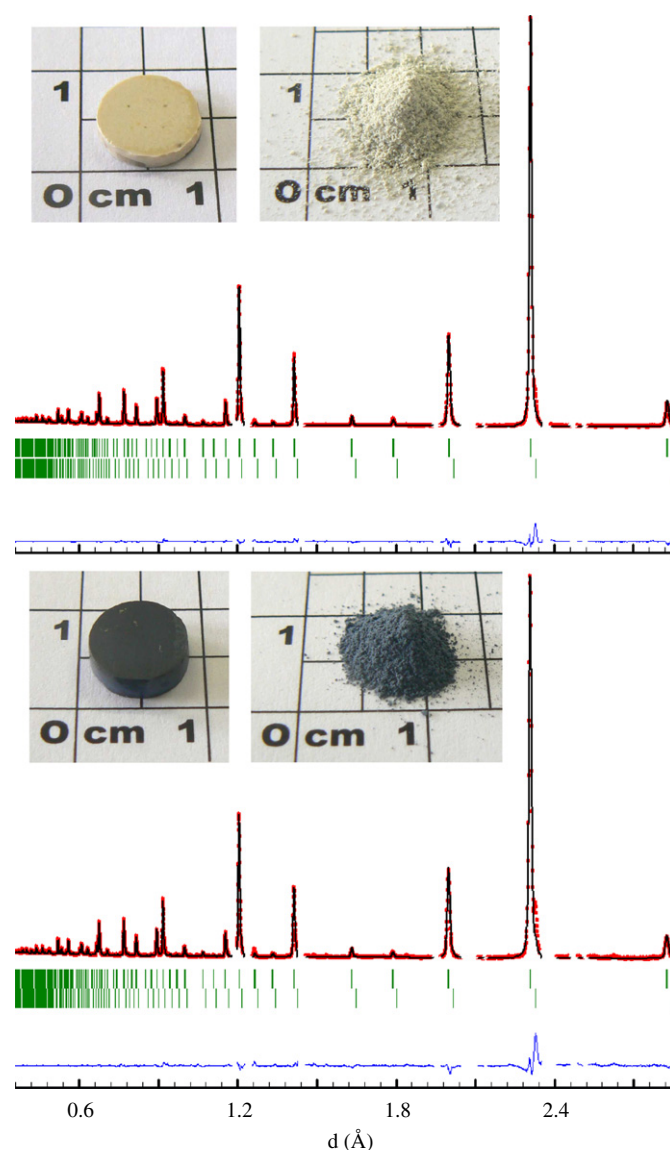

Fig. 4. Neutron diffraction patterns of ground Ba$_{0.95}$La$_{0.05}$TiO$_{3-x}$ nanoceramics (observed=dots, calculated=lines and vertical lines=Bragg peaks with tetragonal phase on top, difference below) reduced after the SPS treatment (bottom) and reoxidized in air (top). Reliability factors: R_p=0.116 and 0.068, R_{wp}=0.115 and 0.072, R_{exp}=0.027 and 0.020, χ^2=18.40 and 12.95. Excluded regions correspond to small amount of impurity phase. Insets show the color of pellets.
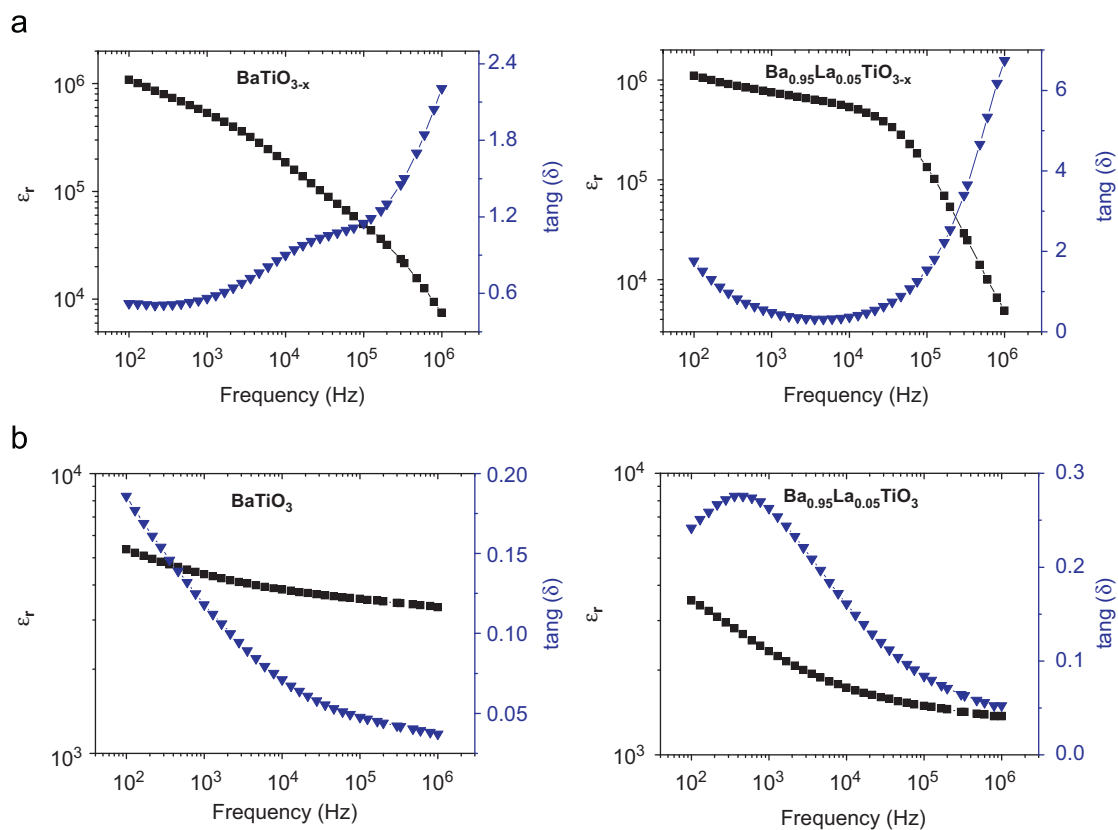
Fig. 5. Room temperature variations of relative permittivities (ε_r) and losses (tan δ) as a function of frequency for (a) SPS sintered ceramics at 1050 °C of $BaTiO_{3-x}$ and $Ba_{0.95}La_{0.05}TiO_{3-x}$ and (b) after oxidation at 850 °C for 50 h.

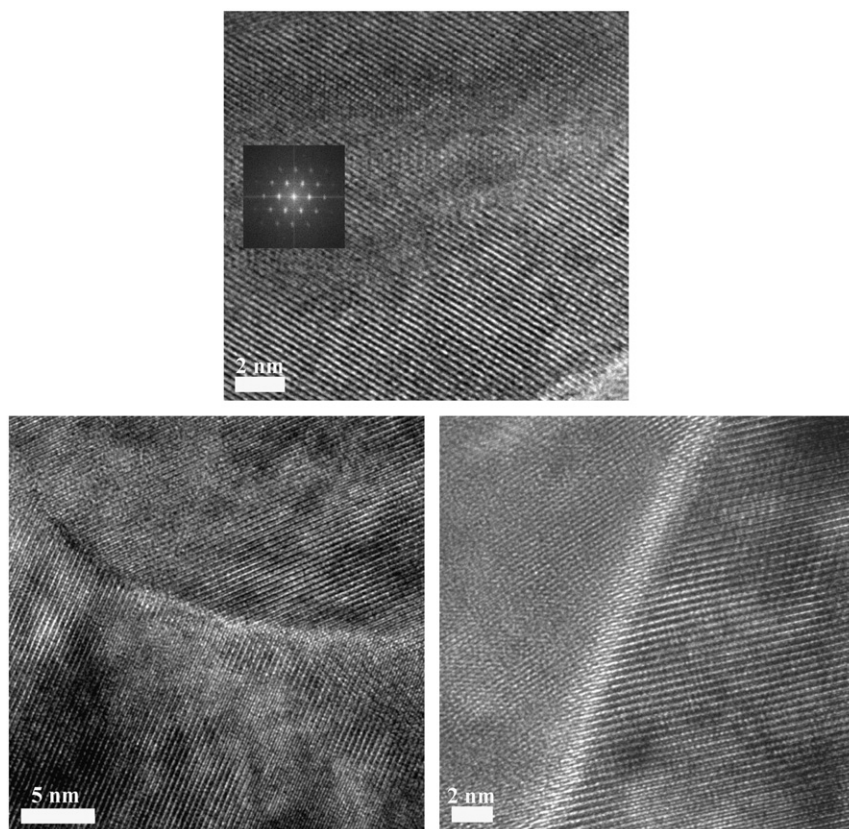**Fig. 6.** HRTEM images of $Ba_{0.95}La_{0.05}TiO_{3-x}$ ceramics sintered at 1050 °C showing unique orientations within each grain (with calculated Fourier transform electron diffraction pattern based on top image) and very fine grain boundaries (bottom).

(Fig. 5a). In these conditions, La-doping preserves the interesting dielectric properties while sintering temperature increases, associated with larger grain size, reduces the capacitive capabilities (and $\tan\delta \geqslant 1$) [16]. Electrode types have no influence on the measured data. Bulk and grain boundary resistances decreases with La-doping and/or increases sintering temperature. Fig. 6 shows HRTEM images of nanosize grains for 5% La-doped $BaTiO_{3-x}$ ceramic sintered at 1050 °C. Such SPS-prepared ceramic, with O deficiency, contains compact nanograins with a unique orientation within each grain, very small grain boundaries (width ~ 1 nm) and low porosity. Activation energies at grain interfaces are very low with $E_a \sim 0.09(2)$ eV. This E_a value is too small to be explained by simple ion movements. The homogeneous and continuous distribution of O, Ti and Ba elements observed across the grain and grain boundary using the EELS technique justifies the low activation energy values (Fig. 7). We believe that the small presence of Ti^{3+} due to sample reduction in SPS apparatus has a strong influence on the dielectric properties measured in our materials. Indeed, all ceramics reheated above 850 °C in air are of white color and show a large decrease of the permittivity values (Fig. 5b). The dielectric properties of nanoceramics can be directly related to the hopping motions of small polarons due to the coexistence of Ti^{4+} and Ti^{3+} within the structure. These results are in very good agreement with those reported by Iguchi et al. [23] for a 0.03 mol% La-doped n-type semiconductor $BaTiO_3$ and other perovskite-related materials with polaron relaxation [24]. Giant permittivities and low E_a values were also reported in hexagonal-$BaTiO_3$ single crystals that show interfacial boundaries consisting of screw dislocations ([25] and references therein). Zhang and Tang [26] explained the dielectric properties determined in $CaCu_3Ti_4O_{12}$, with significantly low activation energy values, by the presence of a polaronic deformation due to the creation of Ti^{3+} ions that distort the lattice with polarons moving along the linked path formed by Ti^{3+}–O–Ti^{4+} bonds. The temperature dependence of the real dielectric permittivity with various frequencies presented in this work is very similar to those shown by other authors [25,26]. The sintering process in SPS apparatus favors the formation of Ti^{3+} due to reducing atmosphere and allows preserving small grain sizes that are individually well crystallized as single domains. The presence of Ti^{3+} associated with O non-stoichiometry appears to be essential in $BaTiO_{3-x}$-type ceramics for the creation of a high number of charges and polaronic conduction. For these materials, we propose that the chemical nature of the dense nanoceramics facilitate the charge transport and an interfacial polarization mechanism to take place through small interfaces that might contribute to relatively low losses and high permittivity values. Although the nature of the interfaces may play a key role in the polarization phenomena, the physical origin of the colossal dielectric constant is not fully understood. Optimization and comprehension of such materials, structures and physical property relationships will be essential for their integration with micro systems to originate more interesting devices and applications.

4. Conclusions

Single-step SPS sintered $BaTiO_{3-x}$ and $Ba_{0.95}La_{0.05}TiO_{3-x}$ ceramics showing colossal permittivity values were structurally characterized. Around fifty nanometer grain size powders prepared by the oxalate route are cubic while tetragonal and cubic phases coexist in nanoceramics after the SPS treatment. For each composition, nanoceramics sintered at 1050 °C present the most interesting electrical features ($\varepsilon \sim 0.8 \times 10^6$ and $\tan\delta < 1$), while permittivity values are lower after sample reoxidition in air. The presence of Ti^{4+} and Ti^{3+}, associated with O (and Ti) vacancies, is considered to participate to the interesting dielectric properties of highly densified nanoceramics via a polaronic conduction mechanism and an interfacial polarization phenomenon. Preparation of ultra-fine and well orientated grains in nanoceramics, and control of a large number of charges at very fine grain interfaces could thus lead to very promising electrical properties for commercial uses in small electronic devices and other integrated systems.

References

[1] L. Wu, Y. Zhu, S. Park, S. Shapiro, J. Tafto, Physical Review B 71 (2005) 014118/1–014118/7.
[2] A.R. West, The Chemical Record 6 (2006) 206–216.
[3] I.P. Raevski, S.A. Prosandeev, A.S. Bogatin, M.A. Malitskaya, L. Jastrabik, Journal of Applied Physics 93 (2003) 41430–44136.
[4] S.B. Desu, D.A. Payne, Journal of the American Ceramic Society 73 (1990) 3416–3421.
[5] M.A.L. Nobre, S. Lanfredi, Journal of Physics and Chemistry of Solids 64 (2003) 2457–2464.
[6] J. Wu, C-W. Nan, Y. Lin, Y. Deng, Physical Review Letters 89 (2002) 217601/1–217601/4.
[7] D.M. Smyth, Journal of Electroceramics 9 (2002) 179–186.
[8] W. Luan, L. Gao, H. Kawaoka, T. Sekino, K. Niihara, Ceramics International 30 (2004) 405–410.
[9] M.T. Buscaglia, M. Viviani, Z. Zhao, V. Buscaglia, P. Nanni, Chemistry of Materials 18 (2006) 4002–4010.
[10] D.C. Sinclair, J.M.S. Skakle, F.D. Morrison, R.I. Smith, T. Beales, Journal of Materials Chemistry 9 (1999) 1327–1331.
[11] W.J. Merz, Physical Review Letters 76 (1949) 1221.
[12] F.D. Morrison, D.C. Sinclair, A.R. West, Journal of Applied Physics 86 (1999) 6355.
[13] R.D. Shannon, Acta Crystallographica A 32 (1976) 751.
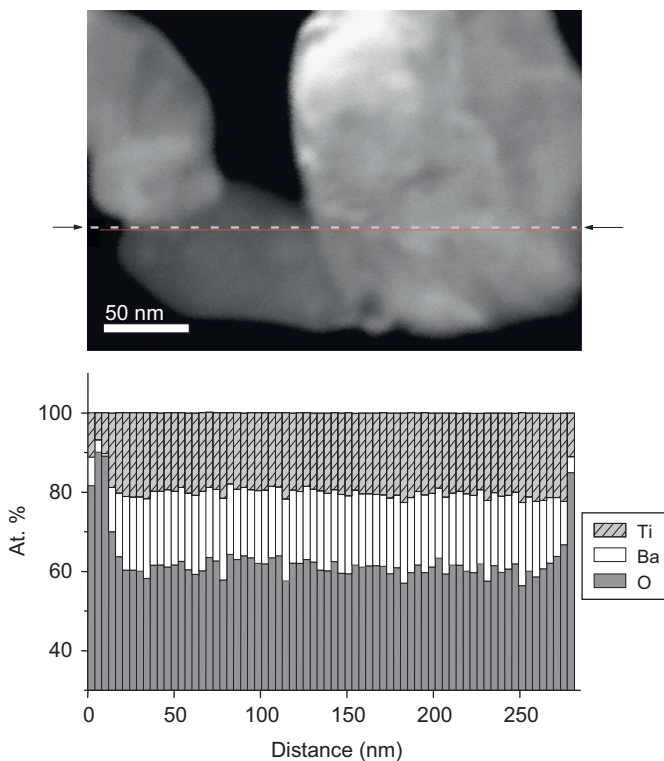[14] F.D. Morrison, A.M. Coats, D.C. Sinclair, A.R. West, Journal of Electroceramics 6 (2001) 219–232.

Fig. 7. Homogeneous distribution of Ba, Ti and O profiles determined by EELS measurements along grain and grain boundaries in $Ba_{0.95}La_{0.05}TiO_{3-x}$ ceramics sintered at 1050 °C (values shown here are essentially qualitative due to the 2.75 nm spot size used for measurements).

[15] A.R. West, T.B. Adams, F.D. Morrison, D.C. Sinclair, Journal of the European Ceramic Society 24 (2004) 1439–1448.

[16] S. Guillemet-Fritsch, Z. Valdez-Nava, C. Tenailleau, T. Lebey, B. Durand, J.Y. Chane-Ching, Advanced Materials 20 (2008) 551–555.

[17] H. Yamamura, A. Watanabe, S. Shirasaki, Y. Moriyoshi, M. Tanada, Ceramics International 11 (1985) 17.

[18] M.T. Buscaglia, V. Buscaglia, M. Viviani, P. Nanni, M. Hanuskova, Journal of the European Ceramic Society 20 (2000) 1997–2007.

[19] T. Takeuchi, M. Tabuchi, H. Kageyama, Y. Suyama, Journal of the American Ceramic Society 82 (1999) 939–943.

[20] G. Busca, V. Buscaglia, M. Leoni, P. Nanni, Chemistry of Materials 6 (1994) 955–961.

[21] S.W. Lu, B.I. Lee, Z.L. Wang, W.D. Samuels, Journal of Crystal Growth 2191 (2000) 269–276.

[22] H.Z. Guo, Z.H. Chen, B.L. Cheng, H.B. Lu, L.F. Liu, Y.L. Zhou, Journal of the European Ceramic Society 25 (2005) 2347–2352.

[23] E. Iguchi, N. Kubota, T. Nakamori, N. Yamamoto, K.J. Lee, Physical Review B 43 (1991) 8646–8649.

[24] O. Bidault, M. Maglione, M. Actis, M. Kchikech, B. Salce, Physical Review B 52 (1995) 4191.

[25] J. Yu, P-F. Paradis, T. Ishikawa, S. Yoda, Y. Saita, M. Itoh, F. Kano, Chemistry of Materials 16 (2004) 3973–3975.

[26] L. Zhang, Z-J Tang, Physical Review B 70 (2004) 174306/1–174306/6.